#### Research Article

Hossein Khorshidi, Chunwei Zhang\*, and Marziyeh Ghasemi

# Alkali-activated binder based on red mud with class F fly ash and ground granulated blast-furnace slag under ambient temperature

https://doi.org/10.1515/rams-2023-0114 received April 10, 2023; accepted August 28, 2023

Abstract: This study examined the fresh and hardened characteristics of alkali-activated binders (AABs) based on ternary mixtures of red mud (RM), class F fly ash (FA), and ground granulated blast-furnace slag (GGBFS). The binders were prepared by dry mixing of 50% RM, 25-50% FA, and 0-25% GGBFS. The alkali activators were prepared from sodium hydroxide solution with different concentrations (6-14 mol) and sodium silicate solution. Curing at room temperature was adopted for the preparation of all samples. The flowability, setting time, and compressive and flexural strength tests were used to examine the properties of the resulting binders. To study the microstructural characterization, the scanning electron microscope, X-ray diffraction, and Fourier transformation infrared techniques were used. The results show that the flowability of the AAB decreases with higher GGBFS content, the addition of GGBFS reduces the setting time, and the incorporation of GGBFS increases the flexural and compressive strengths of the AAB. Microstructural and chemical analysis results indicate that in addition to geopolymer gel, calcium silicate hydrate (C-S-H) is formed upon adding GGBFS, producing a denser microstructure.

**Keywords:** alkali-activated binder, red mud, fly ash, granulated blast-furnace slag, geopolymer, setting time, compressive strength

**Hossein Khorshidi:** School of Marine Science and Engineering, South China University of Technology, Guangzhou 511442, China, e-mail: hossein.khorshidi.m@qmail.com

**Marziyeh Ghasemi:** School of Marine Science and Engineering, South China University of Technology, Guangzhou 511442, China, e-mail: marziyeh.ghasemi.r@gmail.com

#### 1 Introduction

One of the problems of the aluminum industry is red mud (RM). RM remains after the Bayer process in which bauxite ore is digested using caustic soda for alumina production. RM is a hazardous waste as a result of its fineness and high alkalinity, and its disposal is one of the significant environmental problems [1]. RM inventory worldwide is estimated at 4 billion tons, increasing to 150 million tons annually [2]. RM disposal requires a large area of land as well as high management costs. Thus, from economic and environmental viewpoints, adapting a method to reuse RM in a considerable amount is indispensable [3]. Construction and building materials present a valuable opportunity to consume bulk volume of RM [4-9]. Geopolymers, as promising eco-friendly construction materials, could utilize RM as it has silicon and aluminum-containing minerals and high alkalinity [10,11].

Alkali-activated materials (AAMs) are synthesized by polymerization reactions of aluminosilicate precursors such as fly ash (FA), ground granulated blast-furnace slag (GGBFS), waste glass powder, natural pozzolan, RM, and metakaolin (MK) along with alkali activators (e.g., sodium silicate and sodium hydroxide) [12–15]. Geopolymer not only reutilizes industrial byproducts but can also reduce greenhouse gas emission to the environment compared with traditional concrete (which use cement). Geopolymer concrete is superior to Portland concrete in terms of compressive strength, acid resistance, shrinkage, absorption of heavy metals, and excellent potential for improving stability so that it may be a suitable alternative [16].

AAMs are generally divided into two groups based on their calcium content. The first group consists of Ca-rich precursors (class C FA and GGBFS) activated with moderate alkalinity to form C–A–S–H hydration gels. The properties of high-Ca AAMs are shorter setting times, superior early strength, and a greater tendency to crack and shrink [17–19]. Alternatively, the second group contains precursors with low Ca content (*i.e.*, class F FA and MK). These materials, called

<sup>\*</sup> Corresponding author: Chunwei Zhang, School of Marine Science and Engineering, South China University of Technology, Guangzhou 511442, China, e-mail: zhangchunwei@scut.edu.cn

geopolymers, require a high-alkali environment to activate, producing N–A–S–H gels. Low-Ca AAMs can be activated by moderate alkalinity, producing a dense matrix by forming chain-type C–(A)–S–H gels [20–22]. AAMs with high Ca content can generally harden at room temperature since CaO provides more nucleation sites. Low-Ca AAMs, on the other hand, usually require elevated curing temperatures [23].

Over the past years, using RM has received increasing attention in producing geopolymers. Since RM is primarily crystalline and shows low reactivity, good structural properties could not be obtained from pure RM-based geopolymer [9,24]. Thus, most recent studies on the production of RM-based geopolymer materials used it in combination with other aluminosilicate-containing materials, such as FA [25-36], GGBFS [37-41], MK [42-44], and rice husk ash [45,46]. The mechanical properties of RM and class C FAbased geopolymers were investigated by Zhang et al. [26] by analyzing the RM/FA ratio, curing duration, solution/ solid ratio, and sand filler. The samples were activated with residual alkalinity in RM, and added sodium silicate. The compressive strength was reported to be between 7 and 13 MPa, which increased with curing time, and decreased with increasing the RM/FA ratio. Moreover, sand presence in the binder led to a negative effect on mechanical properties. A study by Zhang et al. [25] investigated how the chemical compositions of precursors and curing conditions influenced the mechanical and microstructural properties of geopolymers made of RM and FA. With an RM to FA mass ratio of 1:4, three FA sources were used to prepare the samples. They were activated using a solution of sodium hydroxide and sodium trisilicate. Na/Al and Si/Al molar ratios of 0.6-0.8 and 2, respectively, are suggested as the starting point for synthesizing geopolymers. Results demonstrated that compressive strength ranged from 11.3 to 21.3 MPa in ambient conditions, and up to 180 days of curing could lead to good mechanical properties. Hu et al. [11] produced geopolymers by mixing RM and three types of FA (one class C and two class F) at a ratio of 1:1 and used NaOH and composite solution of NaOH and Na<sub>2</sub>SiO<sub>3</sub> as alkaline reagents. The compressive strengths of RM-class C FA samples that were cured in ambient conditions for 28 days were reported to be 15.2 and 30.3 MPa for activated with the NaOH solution and composite solution, respectively. The CaO in the class C FA composition contributes to the C-S-H formation along with geopolymerization in ambient curing. A NaOH solution alone was not enough to activate the RM-FA geopolymer, even after 2 months of curing in ambient conditions. The results proved that curing at elevated temperatures or activating with a composite activator is essential to acquire adequate compressive strength in the case of RM-class FAbased geopolymer. Lemougna et al. [40] substituted 25-75 wt

% of slag by RM in inorganic polymer systems activated with sodium silicate and cured at 25, 40, and 60°C. As the RM content rose, the reactivity and setting time decreased, and shrinkage increased. The sample with an RM/slag ratio of 50:50 cured at 25°C for 7 days had 54 MPa compressive strength. The highest compressive strength was obtained with a modulus of sodium silicate solution of 2.0. Although using sand and H<sub>2</sub>O<sub>2</sub> led to a decrease in mechanical properties, it introduced the potential utilization of the RM/slag system as mortar and lightweight material. Curing at elevated temperatures and extended time played a crucial role in strength development in a system with high RM content. Bayat et al. [41] investigated the influence of replacing slag with 10-40 wt% RM and 40 wt% thermally treated RM on fresh and hardened properties of alkali-activated slag paste and mortar. The result revealed that using more RM content reduced the fluidity, consistency loss rate, and flexural strength while it increased cohesiveness. The highest compressive strength was reported in 20% RM substitution for slag. The microstructural investigations indicated that the main products were calcium aluminosilicate hydrate (C-A-S-H). and using RM increased the Al incorporation in the paste.

Although there are some studies on AAMs from RM in combination with FA or slag in the literature of research, there still needs to be more research on using FA and GGBFS simultaneously in producing RM-based AAMs. Furthermore, past studies illustrated that the desired mechanical properties of AAM lie in the minor use of RM. In addition, most of the studies reported so far in this field have focused on the development of heat-hardened alkali-activated binders (AABs), which limits their application for in situ casting. AABs produced with ambient temperature curing can be used beyond precast elements, thereby reducing energy and costs associated with elevated temperature curing. Therefore, the aim of this research was to investigate the feasibility of synergistic use of GGBFS and FA in such a way as to enable the significant use of RM in the AAB structure at ambient temperatures. The changes in the effect of sodium hydroxide molarity on the mechanical properties of the binder were also investigated in this study. The RM amount was constant at 50%, and the GGBFS and FA varied from 0 to 25% and 25 to 50% of solid precursors, respectively. Alkaline activators were prepared from sodium silicate and sodium hydroxide composite solutions. The fresh and hardened properties were evaluated by testing the flowability and setting time of the binders along with compressive and flexural strengths. Scanning electron microscopy (SEM), X-ray Diffraction (XRD) analyses, and Fourier transformation infrared (FTIR) were employed to investigate the microstructural characterization.

#### 2 Material and methods

#### 2.1 Solid precursors

RM was obtained from the aluminum company of Xinfa group, Shandong province, China, which was ground and sieved to pass No. 50 sieve (300 µm). Using commercially available class F FA (as defined in ASTM C618 [47]) was considered the primary source of aluminosilicate material. The GGBFS used in this study was kindly provided by Songhe Group, Shandong, China. The solid precursors used in the tests are shown in Figure 1. The specific gravity of materials was obtained following the ASTM C188 [48] test method, and the specific surface area was determined using Blaine's air permeability apparatus, according to ASTM C204 [49] specifications. The particle size distribution (PSD) of the solid precursors were obtained by laser diffraction analysis. The X-ray fluorescence tests were carried out to determine the chemical compositions of precursors. These chemical compositions and physical properties of RM, FA, and GGBFS are presented in Tables 1 and 2. Also, Figures 2-4 show PSD, XRD patterns, and SEM images of raw powder materials, respectively.

Table 2: Physical properties of the RM, FA, and GGBFS (%)

Material	Specific	Gra	ain size	Specific surface		
	gravity	d10	d50	d90	area (m²·cm <sup>−3</sup> )	
RM	3.09	1.10	2.20	4.31	2.883	
FA	2.24	5.68	16.70	35.55	0.379	
GGBFS	2.72	4.56	10.70	21.19	0.600	

As shown in Table 2, since all raw materials contain alumina and silica, they can all be used to prepare AABs. Additionally, RM possesses 32% iron oxide, which is responsible for its rusty appearance. As GGBFS has a high CaO content (35%), it can accelerate the hardening process of the binder and solve the slow reaction rate problem when the binder is cured at ambient conditions.

According to Figure 2, in comparison to the GGBFS and FA, RM has a relatively smaller particle size. FA comprises more large particles among solid precursors. Particle size has a vital role to play in the alkaline solution's initial dissolution since it determines how much surface area is available.

The XRD pattern of the precursors in Figure 3 showed that GGBFS was mainly amorphous with a wide diffuse



Figure 1: Samples of RM, FA, and GGBFS used in the tests.

Table 1: Chemical compositions of solid precursors (%)

Composition(%)								0% 100%					100%							
Material	Fe <sub>2</sub> O <sub>3</sub>	AI203	SiO <sub>2</sub>	Na <sub>2</sub> O	TiO <sub>2</sub>	СаО	<i>SO</i> <sup>3</sup>	P <sub>2</sub> O <sub>5</sub>	MgO	<i>V</i> <sub>2</sub> <i>O</i> <sub>5</sub>	Cr <sub>2</sub> O <sub>3</sub>	ZrO <sub>2</sub>	MnO	Cl	K20	Ono	ZnO	NiO	SrO	BaO
RM	32.03	21.24	14.62	12.10	7.12	4.17	0.61	0.28	0.26	0.18	0.13	0.13	0.09	0.06	0.06	0.01	0.01	94 PPM	94 PPM	0.00
FA	2.33	36.36	53.69	0.52	1.06	2.57	0.46	0.23	0.88	0.00	0.01	0.09	0.02	0.00	1.59	0.01	0.01	68 PPM	0.05	0.10
GGBFS	0.30	15.36	26.17	0.45	2.06	35.29	2.38	0.00	10.74	0.00	0.00	0.06	0.51	0.00	0.27	0.00	0.00	0.00	0.05	0.00

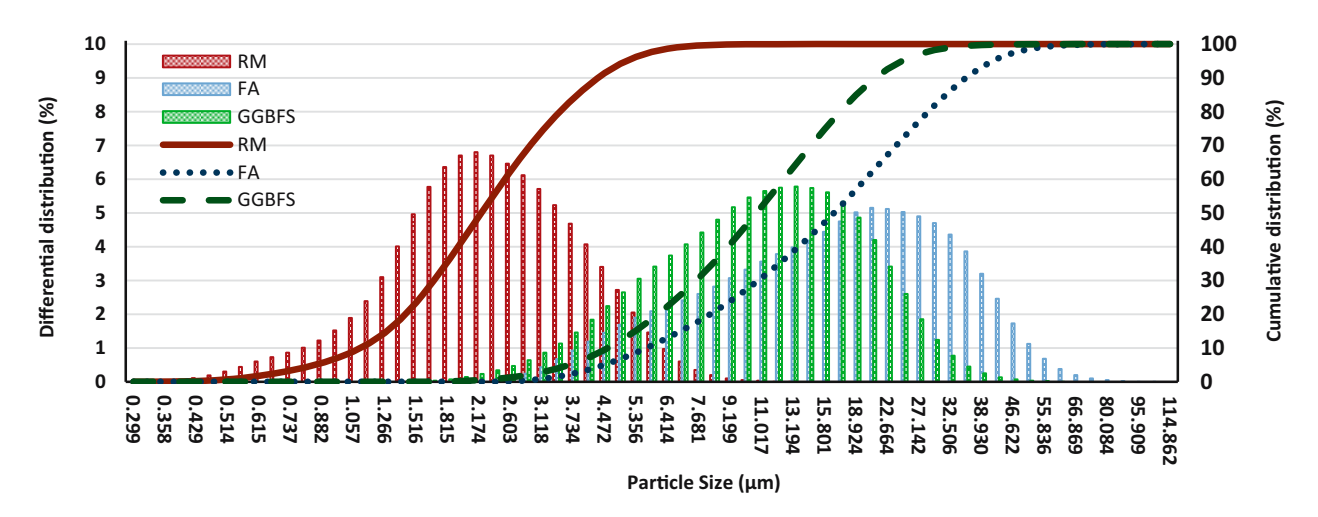


Figure 2: PSD of RM, FA, and GGBFS.

hump at  $23-37^{\circ}(2\theta)$ , and there were some crystalline reflections around 30-33. Meanwhile, the crystalline phases found in RM at room temperature were mainly hematite and lime (CaO). FA is composed primarily of quartz and mullite.

Figure 4 illustrates that FA mainly consisted of solid sphere-like particles and that some particles also contained smaller spheres. Flaky form, rugged texture, and large surface area were some characteristics of the RM particles. There were several lumps with irregular shapes in the RM sample, and these lumps were composed of much smaller particles. Since the composition of the RM mainly consists of hematite, the clusters are probably hematite particles [50]. The microstructure of GGBFS had an irregular polygonal geometry that varied in shape and size and contained large particles with smooth surfaces [51,52].

#### 2.2 Alkali activators

An alkaline solution increases the pH level and eases dissolution by adding alkali cations. The solution extracts Si and Al atoms from the solid precursors to create polymeric Si–O–Al bonds during polymerization. The activator solution was composed of sodium hydroxide and sodium silicate because the NaOH has a great capacity to liberate the silica and alumina monomers, and Na-associated soluble silicates speed up the polymerization process [53].

Sodium hydroxide flakes containing 96% purity and sodium silicate solution containing 8.2% sodium oxide and 26% silicon dioxide and a density of 1.38 g·m<sup>-1</sup> at 20°C were supplied from Sinopharm Chemical Reagent Co., Ltd (Shanghai, China) and Jiashan Yourui Refractory Material Co., Ltd (Jiaxing, China),

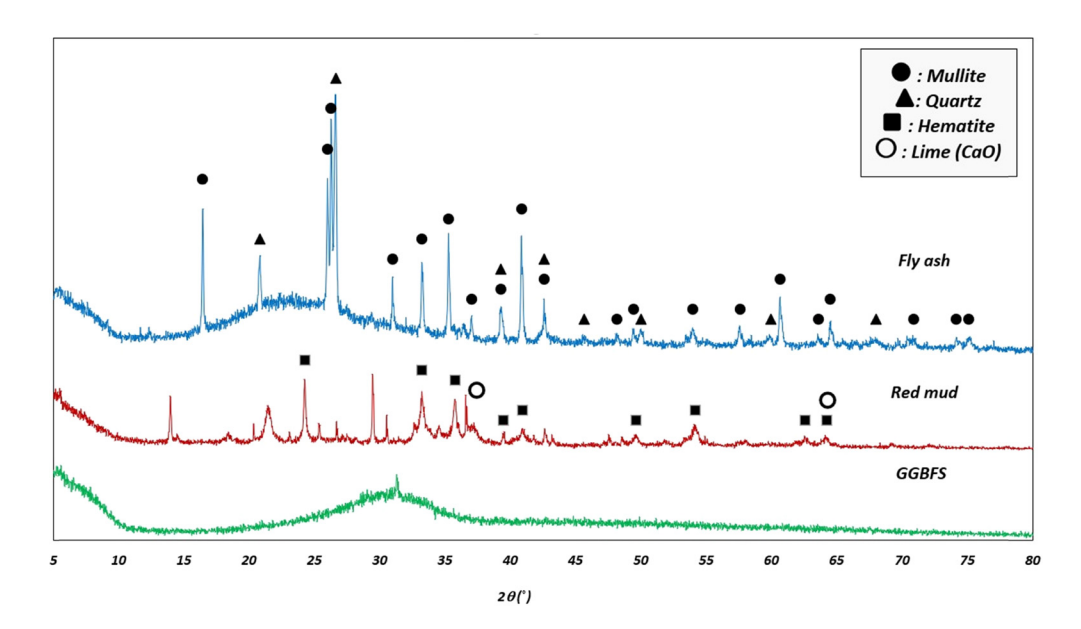


Figure 3: XRD patterns of RM, FA, and GGBFS.

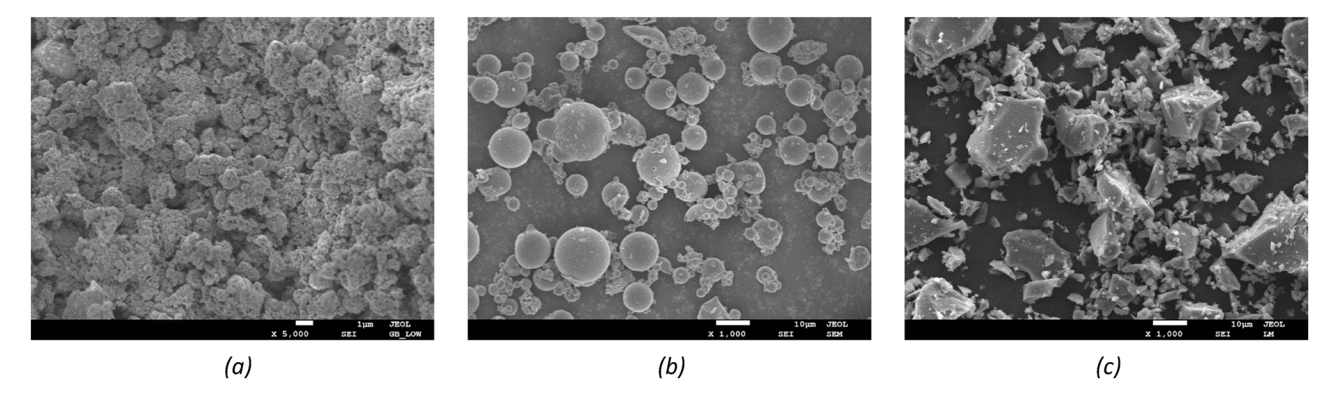


Figure 4: SEM micrographs of (a) RM, (b) FA, and (c) GGBFS.

respectively. For preparing the NaOH solution, first, sodium hydroxide flakes, depending on their molarity, were weighed and then dissolved in tap water using a magnetic stirrer.

The hydroxide solution was used after cooling the exothermically heated liquid to room temperature for about 2 h. A review of previous research suggests that the sodium silicate to sodium hydroxide mass ratio should be 2.0-2.5 for AABs to react more efficiently. In this research, this value is considered constant and equal to 2 [16]. In the required amount, sodium silicate solution was mixed with hydroxide solution to create an alkaline solution. The alkaline solution was prepared 24 h in advance.

#### 2.3 Mix proportion

As mentioned earlier, this study aims to use a large amount of RM (50% of solid precursors) in the AAB structure. In laboratory trials, we found that binary RM and FA systems with a 1:1 ratio and different activator dosages did not achieve sufficient strength, whether cured at room temperature or 60°C. To address this issue, GGBFS was partially substituted for FA. Based on the authors' initial

assessment of ternary binders and previous studies on binary systems based on FA and slag, to achieve a workable mix with acceptable setting time and mechanical properties, the GGBFS content was kept around 20% [54,55]. To determine the optimum content of CaO in solid precursor compositions, FA was replaced with GGBFS at 5, 10, 15, 20, and 25% of the total weight of solid ingredients. In the study, it was decided to use a fixed solution/solid ratio of 0.4 for all of the AABs. First, through fresh and mechanical properties, using RM at a fixed amount of 50% of the total weight of solid precursors, the optimum contents of GGBFS and FA were determined, and then the influence of various NaOH concentrations in composite activators on the optimal mixture from the previous stage was investigated. Table 3 presents the mix proportions of AABs.

## 2.4 Mixing procedure and sample preparation

First, the solid precursors, including RM, GGBFS, and FA, are mixed in the Hobart mixer for 4 min to obtain a homogeneous powder. The composite activator was then added

Table 3: Mixture compositions of AABs used in the present study

Sample ID	RM (%)	FA (%)	GGBFS (%)	NaOH (mol)	Na <sub>2</sub> SiO <sub>3</sub> /NaOH	W/B
R50F50G00-10	50	50	0	10	2	0.4
R50F45G05-10	50	45	5	10	2	0.4
R50F40G10-10	50	40	10	10	2	0.4
R50F35G15-10	50	35	15	10	2	0.4
R50F30G20-10	50	30	20	10	2	0.4
R50F25G25-10	50	25	25	10	2	0.4
R50F30G20-06	50	30	20	6	2	0.4
R50F30G20-08	50	30	20	8	2	0.4
R50F30G20-12	50	30	20	12	2	0.4
R50F30G20-14	50	30	20	14	2	0.4

to the mixture and mixed for two sets of 3 min at low and high speeds. For flexural and compressive strength tests, binders were immediately cast in plastic prism molds of  $40 \times 40 \times 160$  mm; then, an electric vibrator was used to vibrate the specimens for 2 min. Molds were covered with plastic sheets, and the specimens were demolded after  $48\,h$ , sealed with clear polyethylene sheets, and cured at a temperature of  $23 \pm 2^{\circ}\text{C}$ .

## 2.5 Fresh, hardened, and microstructural test methods

The flow value was measured by the ASTM C1437 [56] flow table test. Following mixing, AABs were poured into the cone at the center of the flow table, and the cone was lifted after 1 min. After that, the table was dropped 25 times within 15 s. Then, a ruler was used to determine the flow diameter. The percentage flowability was calculated using the average diameter of the two orthogonal readings as the flow diameter and the cone's internal base diameter. ASTM standard C191 [57] was used for calculating initial and final setting times with the Vicat apparatus. Observations of setting time began with adding the alkaline solution, which activated the aluminosilicate minerals. The initial setting time was defined as the time when the Vicat needle penetrated 33-35 mm into the Vicat Apparatus mold, and the final setting time was defined as the time when the needle made an impression on the AABs, but the annular collar did not. The flexural strength tests were conducted using

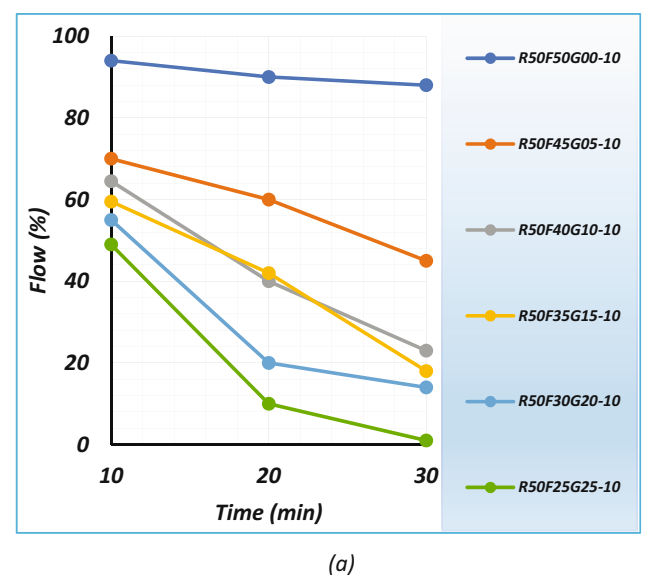
three-point loading as specified in ASTM 348 [58]. The specimens were placed in the center loading system of two load-bearing rods with a clear span of 120 mm. After that, the load-applying rod was brought in contact with the specimens' surface at the third point, and a load was applied until the specimens broke. The compressive strength tests were conducted using the broken prism samples from the flexural strength tests as per ASTM C349 [59] standard procedure. Specimens were tested after 7 and 28 days of curing. The maximum load was recorded on the test samples, and the average strength was taken from the average value of three and six of the test samples for flexural and compressive strength, respectively. Standard deviation is indicated by the error bar in Figures 7 and 8. A diffractometer was used to perform XRD, while SEM was used to evaluate the samples' morphological characteristics. Phase transformations during the processes of decomposition and geopolymerization were investigated with the FTIR test.

#### 3 Results and discussion

#### 3.1 Workability

Figure 5(a) shows the effect of GGBFS addition on the flow of fresh AABs with a solution/solid ratio of 0.4 in 10, 20, and 30 min after adding alkali activator to solid precursors.

The flow of alkali-activated pastes decreased with the increase in the GGBFS content. The results are consistent with previous studies without RM, where mixture with



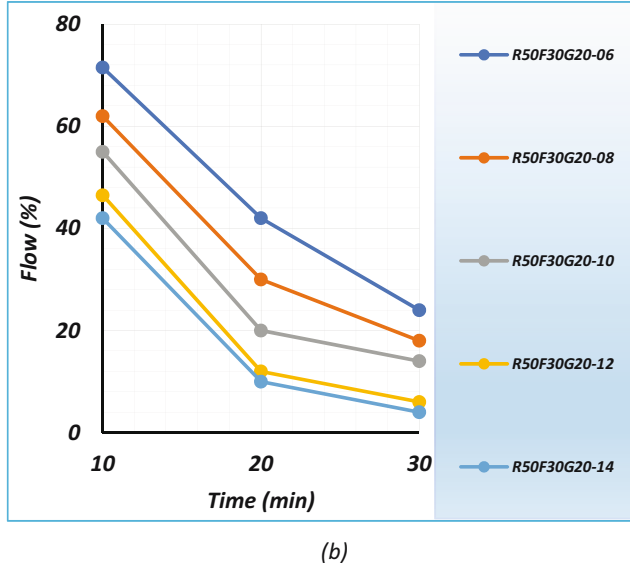
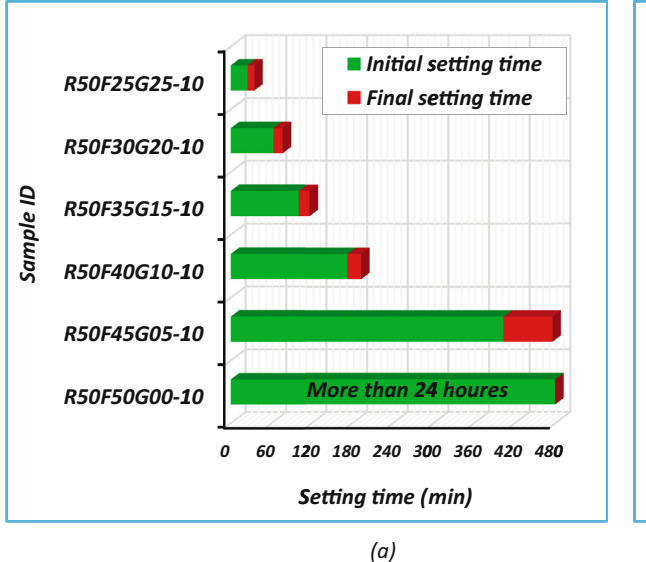


Figure 5: The flow of fresh AABs: (a) effect of GGBFS content and (b) effect of NaOH concentration.



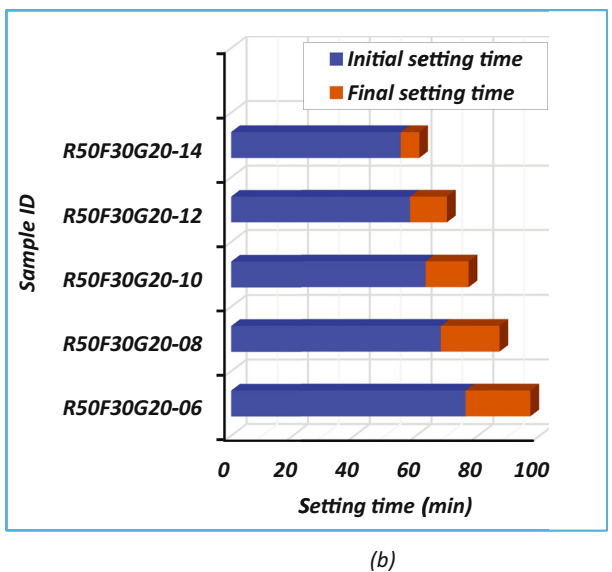
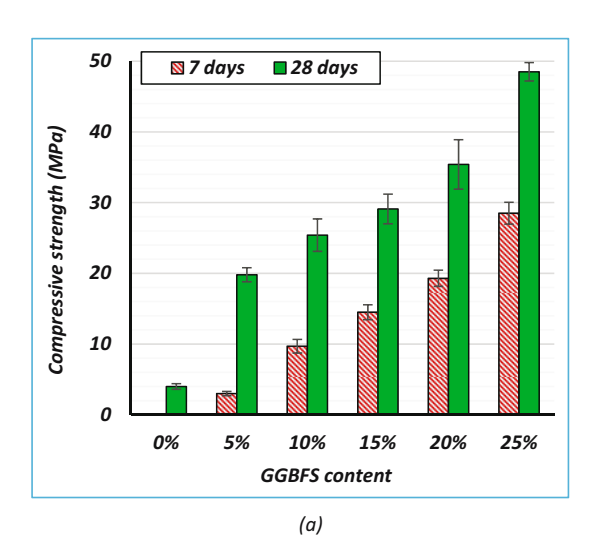


Figure 6: Initial and final setting times of the binders: (a) effect of GGBFS content and (b) effect of NaOH concentration.

lower ratio of GGBFS to FA showed improved flowability [60–63]. This decrease in flow value could be attributed to the angular shape of GGBFS particles in comparison to the spherical FA particles, as shown in Figure 4. The angular particles in the paste matrix increased after FA was replaced by GGBFS, increasing the friction between the particles and thus reducing the paste mobility. A decrease in workability might also be due to the accelerated reaction of GGBFS. In addition, GGBFS has a higher specific surface area than FA, leading to a higher requirement for liquid, resulting in decreased workability [64–67]. The slump value was reduced by 25.6, 31.4, 36.8, 41.5, and 47.9% with the addition of 5, 10, 15, 20, and 25% GGBFS compared to

R50F50G00-10, respectively. As shown in Figure 5(a), the flow of R50F50G00-10 (without GGBFS) showed a slight drop with time up to 30 min, and R50F25G25-10 (with 25% GGBFS) lost its flow after 20 min, and then its flow almost reached zero after 30 min.

Figure 5(b) shows the effect of different concentrations of NaOH in the composite activator on the flow of binders. Increasing the NaOH concentration reduced the binder flowability so that the binder flow values in concentrations of 6, 8, 10, 12, and 14 mol of NaOH were equal to 71.5, 62, 55, 46.5, and 42%, respectively. Also, according to Figure 5(b), with the increase in NaOH concentration, the amount of flow drop increased with time. This could be due to the



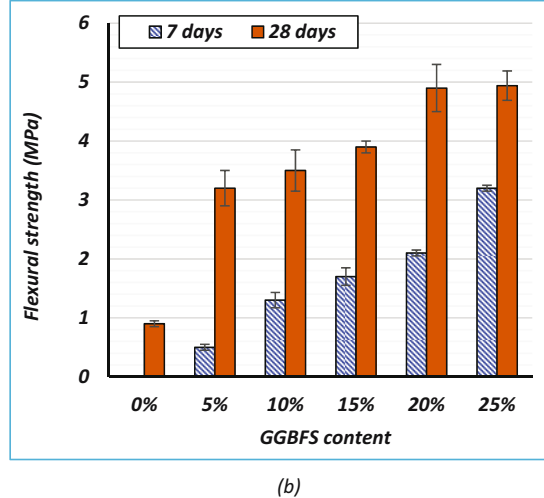


Figure 7: The effect of GGBFS content on AABs: (a) compressive strength and (b) flexural strength.

increase in sodium hydroxide concentration, which raised the pH of the mixture resulting in faster dissolution and greater penetration of SiO<sub>2</sub> and Al<sub>2</sub>O<sub>3</sub>. Thus, accelerating the process of geopolymerization. Furthermore, the higher molarity of NaOH solution has resulted in lower mixture workability due to its higher viscosity [68–70].

Based on the result from the above experiment, it is recommended that superplasticizers or a higher solution/solid ratio be used in the development of mortar and concrete based on RM-based AAB in order to compensate for the high water absorption of RM due to its high specific surface area.t

#### 3.2 Setting time

Setting time is one of the most critical parameters in binding materials. It should be sufficient to allow for appropriate mixing and molding. A long setting time, on the other hand, negatively impacts production efficiency [71]. According to the above explanation, the ASTM C150 standard [72] has considered an acceptable range for the setting time, according to which the setting time should not be less than 45 min and more than 375 min. The initial and final setting times of the binders are presented in Figure 6. The variations in the setting time of binders with various GGBFS content are illustrated in Figure 6(a). As the GGBFS replacing level increased, both the initial and final setting times of binders decreased. In the case of no utilization of GGBFS (R50F50G00-10), the initial and final setting times were more than 24 h.

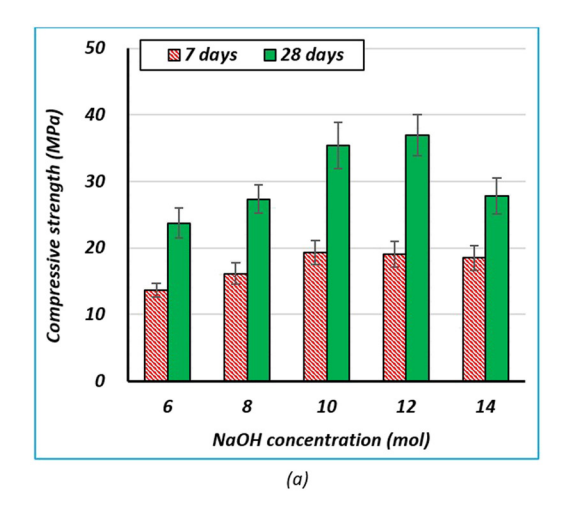
As GGBFS content increased to 25%, the initial and final setting times, and their differences, significantly decreased, so that the initial setting time of the mixture with replacing

of 5, 10, 15, 20, and 25% of GGBFS was equal to 404, 173, 101, 63, and 25 min, respectively. The final setting time was equal to 476, 193, 117, 77, and 35 min, respectively. Samples with higher GGBFS content decreased their setting time by a more significant percentage because C–A–S–H gel and N–A–S–H gel were formed in the early stages due to the corresponding higher amount of reactive GGBFS, which accelerated the reaction process [73] – the setting times of R50F40G10-10, R50F35G15-10, and R50F30G20-10 samples agreed with the ASTM C150 [72] limits.

Alkaline solutions greatly influenced the setting time of AABs. The setting times of binders for different NaOH concentrations are depicted in Figure 6(b). All AABs were observed to set faster when NaOH concentrations were increased from 6 to 14 mol. The initial setting time of R50F30G20 pastes (50% RM, 30% FA, and 20% slag) with NaOH solution concentrations of 6, 8, 10, 12, and 14 mol was equal to 76, 68, 63, 58, and 55 min, respectively. The final setting time was equal to 97, 87, 77, 70, and 61 min, respectively. The reason for this was that the dissolution of aluminate silicate species was improved by higher NaOH concentrations and calcium (sodium) aluminosilicate hydrate (C(N)-A-S-H) gel could be easily formed by accelerated decomposition and hydration of the GGBFS structure in the presence of OH<sup>-</sup> ions from alkaline solutions, thereby enhancing the geopolymerization process and accelerating the setting of the binder [74–76].

#### 3.3 Mechanical properties

Pursuing high compressive strength has been a substantial aim in AAMs development. This is because of the significant characteristic of structural composites sustaining compressive



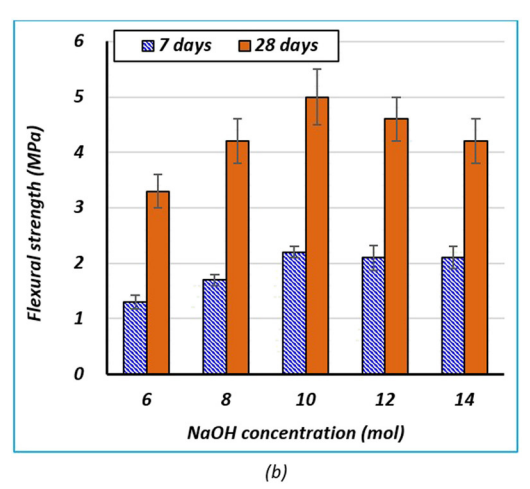


Figure 8: The effect of NaOH concentration on AABs: (a) compressive strength and (b) flexural strength.

forces. The 28 days compressive strength is the main parameter in the concrete design and can be regarded as an indicator for such materials. Moreover, the simplicity of measuring this property and its observed relationship with other properties at the microstructural level contribute to its popularity. Also, flexural strength is the property of the material to withstand energy-induced bending deflection. It is determined as the highest stress that the material demonstrates during failure due to the three points flexural load.

The results of compressive strength and flexural strength tests on samples after 7 and 28 days curing are shown in Table 4 and Figures 7 and 8.

#### 3.3.1 Effect of GGBFS content

It was observed that the mixtures without GGBFS after 7 days were not yet hardened enough and would deform with little pressure. It was due to the slow chemical reaction of silica and alumina contents of FA and RM, as breaking the Si and Al monomers from the FA and RM particles is difficult at ambient temperature. The dissolution of the Si and Al monomers in the alkaline solution is very slow; hence, condensation of the geopolymerization process was not able to initiate at an early age [77]. Thus, flexural and compressive strength tests were performed for these samples only at 28 days.

With the increase in GGBFS content, binders' compressive and flexural strengths at 7 and 28 days increased. In addition, all samples' compressive and flexural strengths increased with the increase in the curing age.

Figure 7(a) illustrates the compressive strength of samples with various GGBFS substitution levels. As can be seen, with the increase in GGBFS content in the mixture, the compressive strength increased at both ages of 7 and 28 days. For example, when the GGBFS content was increased from 0 to 5, 10, 15, 20, and 25% by weight, the compressive strength was increased from almost 0 to 3, 9.7, 14.5, 19.3, and 28.5 MPa at 7 days, and from 4 to 19.8, 25.4, 29.1, 35.4, and 48.5 MPa at 28 days, respectively. The results are consistent with those reported in previous studies [61,78]. It could be explained that with the geopolymer phase, C-S-H and C-A-S-H are formed, reducing the porosity and making the geopolymer paste denser [60,73,79–82]. Furthermore, the heat generated by GGBFS' exothermal reaction with alkaline solutions facilitates geopolymerization. In addition, because this reaction consumes water and increases alkalinity, FA particles dissolve faster, increasing polycondensation [83-85]. Also, according to Figure 7, with the addition of GGBFS, the increase in the rate of strength at the age of 7 days was more than that of 28 days. This was because geopolymer paste with high GGBFS content

Table 4: Flexural and compressive strengths of AABs

Sample ID	Flexura	l strength	Compressive strength				
	7 days	28 days	7 days	28 days			
R50F50G00-10	NT	0.9	NT	4.0			
R50F45G05-10	0.5	3.2	3.0	19.8			
R50F40G10-10	1.3	3.5	9.7	25.4			
R50F35G15-10	1.7	3.9	14.5	29.1			
R50F30G20-10	2.2	4.9	19.3	35.4			
R50F25G25-10	3.2	4.9	28.5	48.5			
R50F30G20-06	1.3	3.3	13.6	23.8			
R50F30G20-08	1.7	4.2	16.1	27.4			
R50F30G20-12	2.1	4.6	19.1	37.0			
R50F30G20-14	2.1	4.2	18.5	27.9			

NT: Not tested.

hydrates faster due to the nucleation effect of Ca<sup>2+</sup>, resulting in higher early-age strength [62,86,87].

Figure 7(b) shows the effects of different GGBFS substitutions on the 7- and 28 days flexural strength of AAB. Similar to compressive strength, the flexural strength of binder samples was also improved by increasing GGBFS content. When the GGBFS content increased from 0 to 5, 10, 15, 20, and 25% by weight, the flexural strength increased from 0 to 0.5, 1.3, 1.7, 2.1, and 3.2 MPa at 7 days and from 0.9 to 3.2, 3.5, 3.9, 4.9, and 4.9 MPa at 28 days, respectively. The reason is the same as that mentioned in the compressive strength discussion. As could be seen, with the increase in the GGBFS replacing level from 20 to 25%, although the 7 days flexural strength increased, the 28 days flexural strength did not change and remained almost constant.

#### 3.3.2 Effect of NaOH concentration

An evaluation of the flexural and compressive strengths of AAB was carried out with solutions containing 6, 8, 10, 12, and 14 mol NaOH in the activator phase. In the activator phase, a mass ratio of sodium silicate to sodium hydroxide was maintained at 2, and based on the results of the first experimental series, the proportion of RM-FA-GGBFS in the solid phase was 50:30:20. The charts in Figure 8 show how the flexural and compressive strengths of the binders' samples depend on the concentration of NaOH in the activator solution.

The highest 7- and 28 days compressive strengths at 10 and 12 mol NaOH were 19.3 and 37 MPa, respectively. The highest 7- and 28 days flexural strengths were in the 10 mol NaOH, which were equal to 2.2 and 4.9 MPa, respectively. Increasing the concentration of the NaOH solution from these optimal values to 14 mol has reduced the compressive and flexural strengths. Although with the increase in NaOH solution concentration from 10 to 12 mol, the 28 days compressive strength increased from 35.4 to 37 MPa; due to this slight increase (4.5%) and considering the fresh properties and flexural strength, the 10 mol NaOH was considered as the optimal concentration. The results showed a non-uniform effect of NaOH concentration on the mechanical properties of the AAB. Increasing NaOH concentration to the optimum value resulted in an increase in flexural and compressive strengths since increased NaOH concentration led to the rise in the dissolution of silica and alumina from the solid precursors. In this case, the SiO<sub>2</sub>/Na<sub>2</sub>O mass ratio increased, resulting in a greater level of polycondensation. In turn, this increases the polymerization of soluble Si and Al species, leading to a more compact gel structure and thus better mechanical properties. Alkalinity increased with an increase in the concentration of the activator, which enhanced the alkaline activation reaction. As a result of the high concentration of OH<sup>-</sup> in the solution, Si<sup>4+</sup> and Al<sup>3+</sup> dissolve faster, while Na<sup>+</sup> acts as a charge-balancing cation in the structure [88–93]. On the other hand, the decrease in flexural and compressive strength with the increase in NaOH concentration beyond the optimal amount was because the dissolution of silica and alumina from solid precursors usually

reaches a steady state under high concentrations of NaOH. This negatively affected the polycondensation process because the SiO<sub>2</sub>/Na<sub>2</sub>O mass ratio decreased as the free NaOH increased, and the dissolved silica and alumina remained almost constant [94]. Another reason could be that the forming of GGBFS products was restrained at high NaOH concentrations. The reaction between Ca<sup>2+</sup> from GGBFS particles and OH<sup>-</sup> from NaOH solution could form a layer of Ca(OH)<sub>2</sub> around the surface of GGBFS particles during alkali activation. The layer of Ca(OH)2 was not thick enough to prevent diffusion of dissolved Ca<sup>2+</sup> from GGBFS particles at low OH<sup>-</sup> concentrations, but Ca(OH)<sub>2</sub> accumulated around the surface of GGBFS particles when the concentration of OH<sup>-</sup> is high, which makes diffusion of dissolved Ca<sup>2+</sup> more difficult. Consequently, the strength decreased because less Ca<sup>2+</sup> was available to react with dissolved Si<sup>4+</sup> and Al<sup>3+</sup> to form the C-A-S-H gel. Due to the thick layers of Ca(OH)<sub>2</sub>, the formation of C-A-S-H gel might also be prevented due to the insufficient space around the GGBFS particles [95,96].

# 3.4 Binder microstructure through SEM analyses

SEM tests were performed on small pieces of samples with different GGBFS content that were tested for 28 days

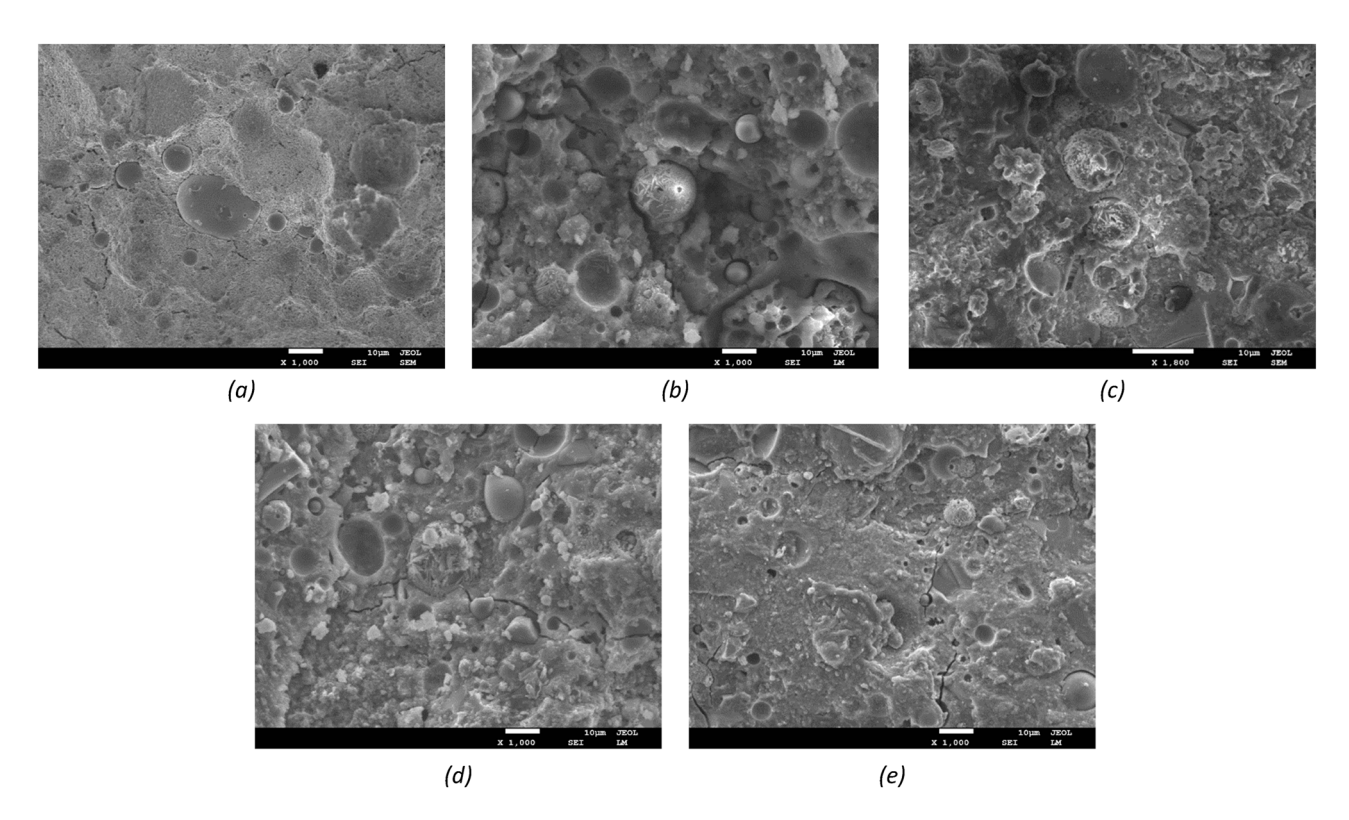


Figure 9: SEM micrographs of (a) R50F50G00-10, (b) R50F45G05-10, (c) R50F4010-10, (d) R50F35G15-10, and (e) R50F30G20-10, at 28 days.

compressive strength. Golden conductive coatings were applied to samples to prevent charging balance. Tests were conducted using the JEOL JSM-7610F model. The SEM images of the AAB samples prepared with 0, 5, 10, 15, and 20% by weight of GGBFS are shown in Figure 9.

When alkali activators were added to the precursors, the active calcium, silicon, and aluminum from the raw materials were dissolved to form C(N)-A-S-H gels. It was also observed that the dissolution of the starting precursor was not complete after alkali activation. Although Al and Si constituted 35% of the RM, substantial amounts of them in the crystalline form provided inert filler to the matrix. Other researchers have also pointed this out [9,11,97]. Also, each mixture contained different amounts of unreacted and/or partially reacted FA and GGBFS particles alongside the alkali activation products. SEM images of samples with different percentages of GGBFS showed that in the sample without GGBFS (R50F50G00-10), there were sponge-like geopolymer gels, and with the increase in GGBFS content in the blends, the sponge-like geopolymer gels could be hardly seen and matrix was denser and more compact. This was because the active calcium in GGBFS can form hydrated products, including C-S-H and C-A-S-H, contributing to the geopolymer network and forming a denser structure. Furthermore, active Ca<sup>2+</sup> acted as a seeding agent for precipitating dissolved precursors and triggering quick hardening at room temperature (as shown in Figure 6(a)) [61]. When GGBFS was utilized, aluminosilicate geopolymerization and heterogeneous nucleation-crystallization appeared to act simultaneously during hardening [11]. Some microcracks were also observed in samples with 15 and 20% GGBFS, possibly caused by shrinkage and quick hydration process [55,98,99]. Moreover, the angular shape of GGBFS (as shown in Figure 4(c)) might contribute to a stronger bond between the particles and the matrix, as well as an enhanced mechanical interlocking that increased microstructure densification [56]. The alteration in AABs' microstructure when GGBFS was added explained the mechanical properties results adequately (Section 3.3.1) and was consistent with the findings of the previous research [54,100].

#### 3.5 XRD analysis of binder

To conduct XRD tests, broken samples remaining after the 28 days compressive strength tests were ground into

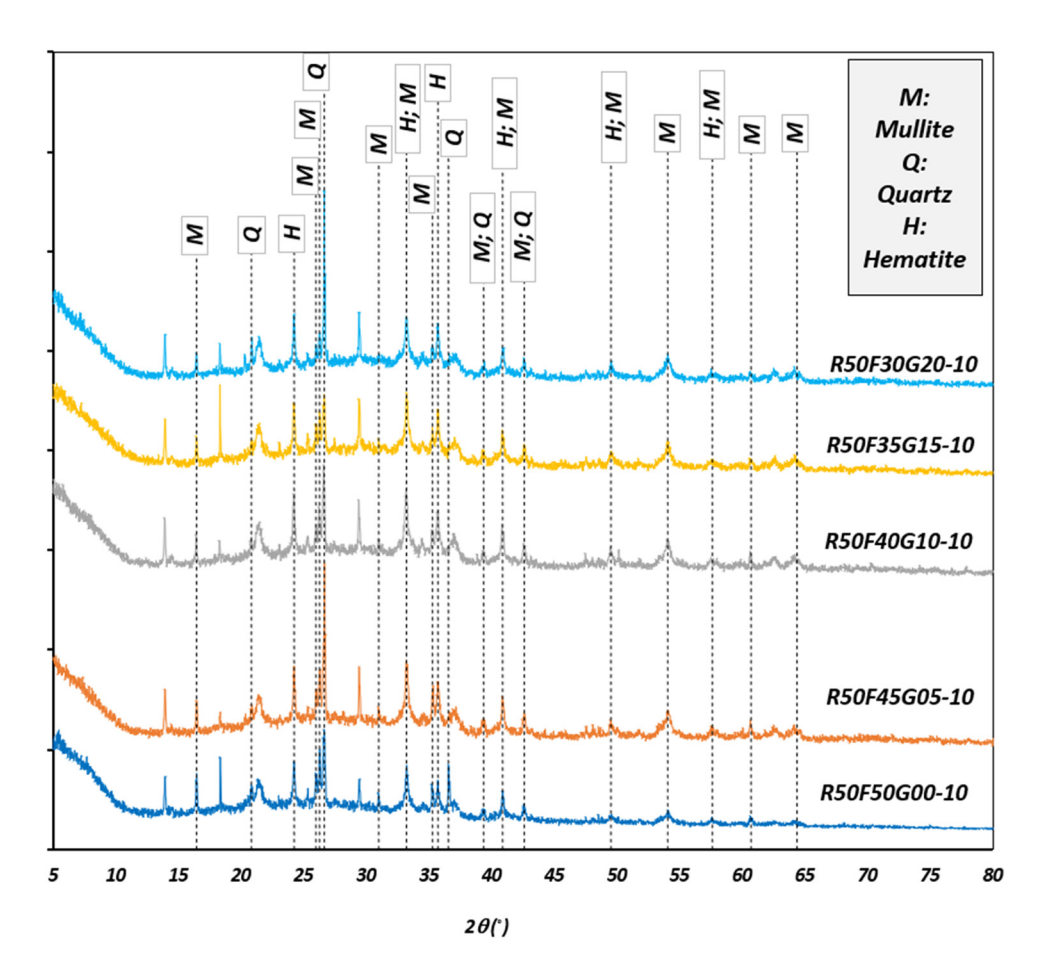


Figure 10: XRD patterns of the binders at 28 days.

powders and sieved to pass the No. 200 sieve (75 µm). It was conducted using a Cu anode. The scanning step size was 0.02°, and its range was 5-80°. The XRD patterns of alkaliactivated pastes with different GGBFS content at 28 days are presented in Figure 10. According to the pattern of precursors in Figure 3, it was observed that after alkali activation, there was no formation of new crystalline phases. In this way, the newly formed phase could be described as amorphous. It is also important to note that the original crystalline reflections of the raw material were also present in the final product, which indicated that these crystalline phases were difficult to dissolve in alkaline conditions. Additionally, XRD analysis revealed that the addition of GGBFS to the AAB blend reduced the intensity of crystalline reflections due to the relatively amorphous nature of slag and the products of alkaline activation of these ternary systems (RM-FA-GGBFS) [71].

### 3.6 FTIR analysis

The FTIR test was performed on the samples prepared according to the XRD section to study phase transformation during the decomposition and alkali activation processes. The FTIR spectrums of AABs containing 0–20% GGBFS after 28 days are depicted in Figure 11. It could be seen that regardless of the GGBFS content, absorption bands were generally found in similar locations on all specimens. The bands at 1,645 and 3,436 cm<sup>-1</sup> in all samples resulted from H–O–H bending vibrations and O–H stretching vibrations

of molecular H<sub>2</sub>O that were absorbed on the surfaces of alkali activation products or entrapped inside their cavities [101–103]. All mixtures exhibited absorption bands at around 1,420 cm<sup>-1</sup>, which indicated O–C–O stretching vibrations in carbonates [24,104]. The high alkaline activator aqueous phase has been atmospherically carbonated, which was diffused on the surface of geopolymeric materials [105,106]. All mixes showed the main absorption band representing the Si–O bond around 996 cm<sup>-1</sup>. The asymmetric stretching vibration of the non-bridging Si–O bonds was attributed to this band, indicating that a chain-structured C–A–S–H gel was predominant in the product [107,108]. The region with the wavenumber of about 460 cm<sup>-1</sup> was characteristic of the deformation stretching of Si–O–Si and O–Si–O [109–111].

#### 3.7 Potential applications of the RMbased AAMs

High-temperature curing has become the primary constraint for using AAMs in cast-*in-situ* applications. For AAMS to be widely used in the construction industry, overcoming this limitation of curing at elevated temperatures is essential. Also, curing without high temperatures reduces costs by avoiding thermal activation. RM-based AAMs evaluated in this study were cured at ambient temperature and had 28 days compressive strength of 4–48.5 MPa, comparable with Portland cement, which has a strength ranging from 9 to 24 MPa [45]. Consequently, these composites are

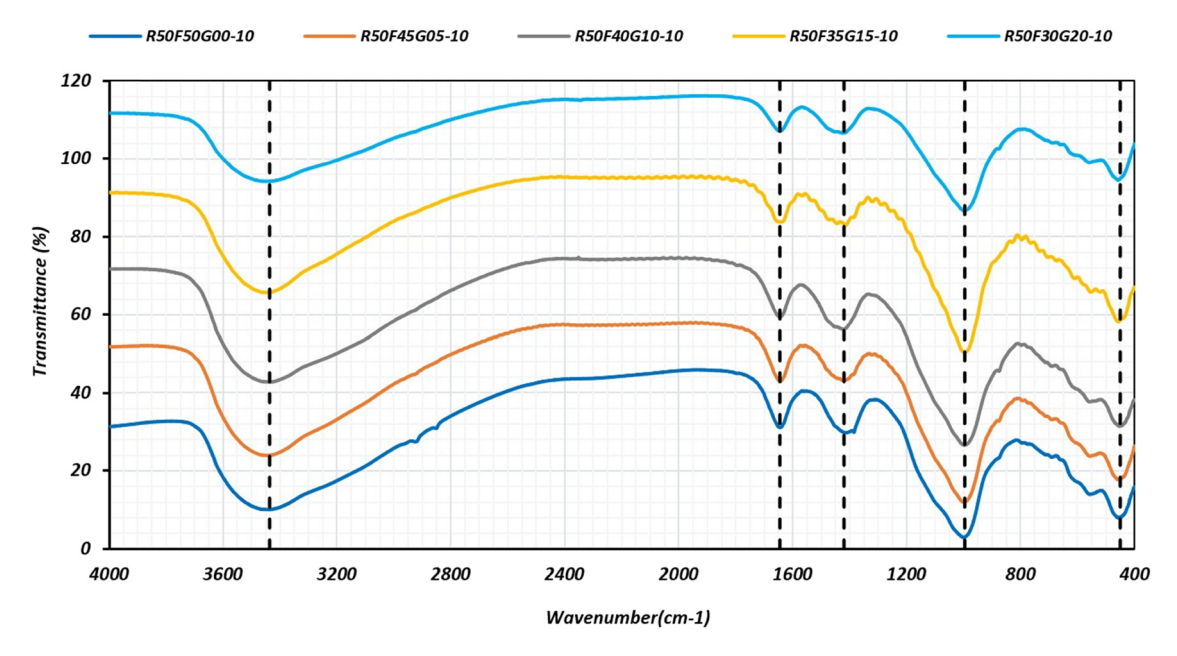


Figure 11: FTIR spectra of the binders at 28 days.

suitable for use as cementitious materials in specific civil engineering applications, including the construction of roads [112-114], and use as building materials such as bricks [2,27,50,115,116], ceramics [24,117-120], thermal and sound insulation [121,122], paving blocks [34], mortar, and lightweight materials [40]. Also, RM has a reddish-colored pigment due to the presence of iron oxide in the composition and can be used to produce colored architectural concrete for aesthetic purposes [123].

### 4 Conclusion

In this study, by utilizing RM, class F FA, and GGBFS, AABs with satisfactory mechanical properties were produced at ambient temperature. Systematic experimental studies have been conducted to determine the optimal GGBFS content and NaOH concentration in composite alkali activators to modify the workability, setting time, and mechanical properties of RM-based AAB. The following are the conclusions drawn from the study:

- · The flow of alkali-activated pastes decreased with the increase in the GGBFS content due to the higher specific surface area and angular shape of GGBFS. Increasing the NaOH concentration accelerated the geopolymerization processes and reduced the binder flowability.
- Increasing the GGBFS replacement level reduced the binders' initial and final setting times. The initial and final setting times of all AABs also decreased with the increased NaOH concentration.
- The compressive and flexural strengths of binders at 7 and 28 days increased with the increase in the GGBFS content. It could be explained that due to the formation of calcium silicate hydrates (C-S-H) and calcium aluminosilicate hydrates (C-A-S-H) along with the geopolymer phase (N-A-S-H), the porosity was reduced, which led to a denser geopolymer paste.
- The optimum replacement rate was 20% FA with GGBFS based on the binders' fresh and mechanical properties assessment. In addition, 10 mol of NaOH concertation was optimal in RM:FA:GGBFS blends with ratios of 50:30:20.
- · The RM used in this study was mainly crystalline and was composed of aluminum and silicon-containing minerals, showed low reactivity, and served as an inert filler. Furthermore, the intrinsic alkalinity of the RM provided alkalis for AAM formation.
- The performance of RM as a component of the alkaline active binder has been satisfactory. Reusing RM in large quantities in construction projects will be environmentally beneficial.

Acknowledgments: The authors are grateful for the reviewer's valuable comments that improved the manuscript.

Funding information: This research is financially supported by the Ministry of Science and Technology of China (Grant No. 2019YFE0112400), the Department of Science and Technology of Shandong Province (Grant No. 2021CXGC011204), the Liaoning Provincial Key Laboratory of Safety and Protection for Infrastructure Engineering, and the Central Government -Liaoning provincial discovery project.

**Author contributions:** All authors have accepted responsibility for the entire content of this manuscript and approved its submission.

**Conflict of interest:** The authors state no conflict of interest.

Data availability statements: All data generated or analysed during this study are included in this published article.

#### References

- Ye, N., Y. Chen, J. Yang, S. Liang, Y. Hu, B. Xiao, et al. Co-disposal of [1] MSWI fly ash and Bayer red mud using an one-part geopolymeric system. Journal of Hazardous Materials, Vol. 318, 2016, pp. 70-78.
- [2] Arroyo, F., Y. Luna-Galiano, C. Leiva, L. F. Vilches, and C. Fernández-Pereira. Environmental risks and mechanical evaluation of recycling red mud in bricks. Environmental Research, Vol. 186, No. Nov 2019, 2020, id. 109537.
- [3] Chen, S., Z. Du, Z. Zhang, D. Yin, F. Feng, and J. Ma. Effects of red mud additions on gangue-cemented paste backfill properties. Powder Technology, Vol. 367, 2020, pp. 833-840.
- Khairul, M. A., J. Zanganeh, and B. Moghtaderi. The composition, recycling and utilisation of Bayer red mud. Resources, Conservation and Recycling, Vol. 141, No. Nov 2018, 2019, pp. 483-498.
- Klauber, C., M. Gräfe, and G. Power. Bauxite residue issues: II. options for residue utilization. Hydrometallurgy, Vol. 108, No. 1-2, 2011, pp. 11-32.
- Mahinroosta, M., Z. Karimi, and A. Allahverdi. Recycling of red mud for value-added applications: A comprehensive review. In: Hashmi S, Choudhury IA, editors. Encyclopedia of renewable and sustainable materials, Elsevier Ltd, Amsterdam, Netherlands, 2020, pp. 561-582.
- [7] Liu, X. and N. Zhang. Utilization of red mud in cement production: A review. Waste Management and Research, Vol. 29, No. 10, 2011, pp. 1053-1063.
- Power, G., M. Gräfe, and C. Klauber. Bauxite residue issues: I. [8] Current management, disposal and storage practices. Hydrometallurgy, Vol. 108, No. 1-2, 2011, pp. 33-45.
- [9] Hertel, T. and Y. Pontikes. Geopolymers, inorganic polymers, alkali-activated materials and hybrid binders from bauxite residue (red mud) - Putting things in perspective. Journal of Cleaner Production, Vol. 258, 2020, id. 120610.

- [10] Singh, S., M. U. Aswath, and R. V. Ranganath. Effect of mechanical activation of red mud on the strength of geopolymer binder. Construction and Building Materials, Vol. 177, 2018, pp. 91–101.
- [11] Hu, W., Q. Nie, B. Huang, X. Shu, and Q. He. Mechanical and microstructural characterization of geopolymers derived from red mud and fly ashes. *Journal of Cleaner Production*, Vol. 186, 2018, pp. 799–806.
- [12] Zhang, P., Z. Gao, J. Wang, J. Guo, S. Hu, and Y. Ling. Properties of fresh and hardened fly ash/slag based geopolymer concrete: A review. *Journal of Cleaner Production*, Vol. 270, 2020, id. 122389.
- [13] Xiao, R., X. Jiang, M. Zhang, P. Polaczyk, and B. Huang. Analytical investigation of phase assemblages of alkali-activated materials in CaO-SiO<sub>2</sub>-Al<sub>2</sub>O<sub>3</sub> systems: The management of reaction products and designing of precursors. *Materials & Design*, Vol. 194, 2020, id. 108975.
- [14] Xiao, R., X. Jiang, Y. Wang, Q. He, and B. Huang. Experimental and thermodynamic study of alkali-activated waste glass and calcium sulfoaluminate cement blends: Shrinkage, efflorescence potential, and phase assemblages. *Journal of Materials in Civil Engineering*, Vol. 33, No. 11, 2021, pp. 1–14.
- [15] Xiao, R., Z. Shen, R. Si, P. Polaczyk, Y. Li, H. Zhou, et al. Alkaliactivated slag (AAS) and OPC-based composites containing crumb rubber aggregate: Physico-mechanical properties, durability and oxidation of rubber upon NaOH treatment. *Journal of Cleaner Production*, Vol. 367, No. Apr, 2022, id. 132896.
- [16] Ng, C., U. J. Alengaram, L. S. Wong, K. H. Mo, M. Z. Jumaat, and S. Ramesh. A review on microstructural study and compressive strength of geopolymer mortar, paste and concrete. *Construction and Building Materials*, Vol. 186, 2018, pp. 550–576.
- [17] Davidovits, J. Why Alkali-Activated Materials (AAM) are NOT Geopolymers? Tech Pap #25, Geopolymer Inst Libr. 2018; (November)
- [18] Nodehi, M. and V. M. Taghvaee. Alkali-activated materials and geopolymer: A review of common precursors and activators addressing circular economy. *Circular Economy and Sustainability*, Vol. 2, No. 1, 2022, pp. 165–196.
- [19] Zhang, C., H. Khorshidi, E. Najafi, and M. Ghasemi. Fresh, mechanical and microstructural properties of alkali-activated composites incorporating nanomaterials: A comprehensive review. *Journal of Cleaner Production*, Vol. 384, No. Oct 2022, 2023, id. 135390.
- [20] Mastali, M., P. Kinnunen, A. Dalvand, R. Mohammadi Firouz, and M. Illikainen. Drying shrinkage in alkali-activated binders – A critical review. *Construction and Building Materials*, Vol. 190, 2018, pp. 533–550.
- [21] Humad, A. M., A. Kothari, J. L. Provis, and A. Cwirzen. The effect of blast furnace slag/fly ash ratio on setting, strength, and shrinkage of alkali-activated pastes and concretes. Frontiers in Materials, Vol. 6, No. Feb, 2019, pp. 1–10.
- [22] Xie, T. and C. Fang. Nanomaterials applied in modifications of geopolymer composites: A review. *Australian Journal of Civil Engineering*, Vol. 17, No. 1, 2019, pp. 32–49.
- [23] Xiao, R., B. Huang, H. Zhou, Y. Ma, and X. Jiang. A state-of-the-art review of crushed urban waste glass used in OPC and AAMs (geopolymer): Progress and challenges. *Cleaner Materials*, Vol. 4, No. Feb, 2022, id. 100083.
- [24] Lemougna, P. N., K. T. Wang, Q. Tang, and X. M. Cui. Synthesis and characterization of low temperature (<800°C) ceramics from red mud geopolymer precursor. *Construction and Building Materials*, Vol. 131, 2017, pp. 564–573.

- [25] Zhang, M., T. El-Korchi, G. Zhang, J. Liang, and M. Tao. Synthesis factors affecting mechanical properties, microstructure, and chemical composition of red mud-fly ash based geopolymers. *Fuel*, Vol. 134, No. Jun, 2014, pp. 315–325.
- [26] Zhang, G., J. He, and R. P. Gambrell. Synthesis, characterization, and mechanical properties of red mud-based geopolymers. *Transportation Research Record*, Vol. 2167, 2010, pp. 1–9.
- [27] Kim, S. Y., Y. Jun, D. Jeon, and J. E. Oh. Synthesis of structural binder for red brick production based on red mud and fly ash activated using Ca(OH)<sub>2</sub> and Na<sub>2</sub>CO<sub>3</sub>. *Construction and Building Materials*, Vol. 147, 2017, pp. 101–116.
- [28] Choo, H., S. Lim, W. Lee, and C. Lee. Compressive strength of onepart alkali activated fly ash using red mud as alkali supplier. Construction and Building Materials, Vol. 125, 2016, pp. 21–28.
- [29] Zhang, M., M. Zhao, G. Zhang, D. Mann, K. Lumsden, and M. Tao. Durability of red mud-fly ash based geopolymer and leaching behavior of heavy metals in sulfuric acid solutions and deionized water. *Construction and Building Materials*, Vol. 124, 2016, pp. 373–382.
- [30] Zhao, M., G. Zhang, K. W. Htet, M. Kwon, C. Liu, Y. Xu, et al. Freezethaw durability of red mud slurry-class F fly ash-based geopolymer: Effect of curing conditions. *Construction and Building Materials*, Vol. 215, 2019, pp. 381–390.
- [31] Yang, Z., R. Mocadlo, M. Zhao, R. D. Sisson, M. Tao, and J. Liang. Preparation of a geopolymer from red mud slurry and class F fly ash and its behavior at elevated temperatures. *Construction and Building Materials*, Vol. 221, 2019, pp. 308–317.
- [32] Koshy, N., K. Dondrob, L. Hu, Q. Wen, and J. N. Meegoda. Mechanical Properties of Geopolymers Synthesized from Fly Ash and Red Mud under Ambient Conditions. *Crystals*, Vol. 9, 2019, id. 572.
- [33] Samal, S., A. K. Ray, and A. Bandopadhyay. Characterization and microstructure observation of sintered red mud-fly ash mixtures at various elevated temperature. *Journal of Cleaner Production*, Vol. 101, 2015, pp. 368–376.
- [34] Kumar, A. and S. Kumar. Development of paving blocks from synergistic use of red mud and fly ash using geopolymerization. Construction and Building Materials, Vol. 38, 2013, pp. 865–871.
- [35] Mucsi, G., R. Szabó, Á. Rácz, F. Kristály, and S. Kumar. Combined utilization of red mud and mechanically activated fly ash in geopolymers. *Rudarsko-geološko-naftni zbornik (The Mining-Geological-Petroleum Engineering Bulletin)*, Vol. 34, No. 1, 2019, pp. 27–36.
- [36] Zhang, M., M. Zhao, G. Zhang, J. M. Sietins, S. Granados-Focil, M. S. Pepi, et al. Reaction kinetics of red mud-fly ash based geopolymers: Effects of curing temperature on chemical bonding, porosity, and mechanical strength. *Cement and Concrete Composites*, Vol. 93, No. Jul, 2018, pp. 175–185.
- [37] Li, S., J. Zhang, Z. Li, Y. Gao, and C. Liu. Feasibility study of red mud-blast furnace slag based geopolymeric grouting material: Effect of superplasticizers. *Construction and Building Materials*, Vol. 267, 2021, id. 120910.
- [38] Singh, S. P., S. Samantasinghar, and D. Sindhuja. Stabilization of red mud using ground granulated blast furnace slag by geopolymerization technique. In: Singh DN, Galaa A, editors. Contemporary Issues in Geoenvironmental Engineering. Springer International Publishing, Cham, 2018, pp. 338–350.
- [39] Liang, X. and Y. Ji. Experimental study on durability of red mudblast furnace slag geopolymer mortar. *Construction and Building Materials*, Vol. 267, 2021, id. 120942.

- [40] Lemougna, P. N., K. T. Wang, Q. Tang, and X. M. Cui. Study on the development of inorganic polymers from red mud and slag system: Application in mortar and lightweight materials. Construction and Building Materials, Vol. 156, 2017, pp. 486-495.
- [41] Bayat, A., A. Hassani, and A. A. Yousefi. Effects of red mud on the properties of fresh and hardened alkali-activated slag paste and mortar. Construction and Building Materials, Vol. 167, 2018, pp. 775-790.
- [42] Hajjaji, W., S. Andrejkovičová, C. Zanelli, M. Alshaaer, M. Dondi, J. A. Labrincha, et al. Composition and technological properties of geopolymers based on metakaolin and red mud. Materials & Design, Vol. 52, 2013, pp. 648-654.
- Kaya, K. and S. Soyer-Uzun. Evolution of structural characteristics and compressive strength in red mud-metakaolin based geopolymer systems. Ceramics International, Vol. 42, No. 6, 2016, pp. 7406-7413.
- He, J., J. Zhang, Y. Yu, and G. Zhang. The strength and micro-[44] structure of two geopolymers derived from metakaolin and red mud-fly ash admixture: A comparative study. Construction and Building Materials, Vol. 30, 2012, pp. 80-91.
- He, J., Y. Jie, J. Zhang, Y. Yu, and G. Zhang. Synthesis and char-[45] acterization of red mud and rice husk ash-based geopolymer composites. Cement and Concrete Composites, Vol. 37, No. 1, 2013, pp. 108-118.
- [46] Sékou, T., D. Siné, T. D. Lanciné, and C. Bakaridjan. Synthesis and characterization of a red mud and rice husk based geopolymer for engineering applications. Macromolecular Symposia, Vol. 373, No. 1, 2017, pp. 1-11.
- [47] ASTM C618-19. Standard Specification for Coal Fly Ash and Raw or Calcined Natural Pozzolan for Use in Concrete. ASTM International, West Conshohocken, PA, 2019.
- ASTM C188-17. Standard Test Method for Density of Hydraulic Cement. ASTM International, West Conshohocken, PA, 2017.
- [49] ASTM C204-16. Standard Test Methods for Fineness of Hydraulic Cement by Air-Permeability Apparatus. ASTM International, West Conshohocken, PA, 2016.
- [50] Singh, S., M. U. Aswath, and R. V. Ranganath. Performance assessment of bricks and prisms: Red mud based geopolymer composite. Journal of Building Engineering, Vol. 32, No. Jan, 2020, id. 101462.
- Sabzi, J., E. A. Shamsabadi, M. Ghalehnovi, S. A. Hadigheh, [51] A. Khodabakhshian, and J. de Brito. Mechanical and durability properties of mortars incorporating red mud, ground granulated blast furnace slag, and electric arc furnace dust. Applied Sciences, Vol. 11, 2021, id. 4110.
- [52] Narimani Zamanabadi, S., S. A. Zareei, P. Shoaei, and F. Ameri. Ambient-cured alkali-activated slag paste incorporating microsilica as repair material: Effects of alkali activator solution on physical and mechanical properties. Construction and Building Materials, Vol. 229, 2019, id. 116911.
- Elahi, M. M. A., M. M. Hossain, M. R. Karim, M. F. M. Zain, and C. [53] Shearer. A review on alkali-activated binders: Materials composition and fresh properties of concrete. Construction and Building Materials, Vol. 260, 2020, id. 119788.
- [54] Yousefi Oderji, S., B. Chen, M. R. Ahmad, and S. F. A. Shah. Fresh and hardened properties of one-part fly ash-based geopolymer binders cured at room temperature: Effect of slag and alkali activators. Journal of Cleaner Production, Vol. 225, 2019, pp. 1–10.
- Lee, N. K. and H. K. Lee. Setting and mechanical properties of alkali-activated fly ash/slag concrete manufactured at room

- temperature. Construction and Building Materials, Vol. 47, 2013, pp. 1201-1209.
- [56] ASTM C1437-15. Standard Test Method for Flow of Hydraulic Cement Mortar. ASTM International, West Conshohocken, PA, 2015.
- [57] ASTM C191-13. Standard Test Methods for Time of Setting of Hydraulic Cement by Vicat Needle. ASTM International, West Conshohocken, PA, 2013.
- [58] ASTM C348-14. Standard Test Method for Flexural Strength of Hydraulic-Cement Mortars. ASTM International, West Conshohocken, PA, 2014.
- [59] ASTM C349-14. Standard Test Method for Compressive Strength of Hydraulic-Cement Mortars (Using Portions of Prisms Broken in Flexure). ASTM International, West Conshohocken, PA, 2014.
- [60] Fang, G., W. K. Ho, W. Tu, and M. Zhang, Workability and mechanical properties of alkali-activated fly ash-slag concrete cured at ambient temperature. Construction and Building Materials, Vol. 172, 2018, pp. 476-487.
- [61] Nath, P. and P. K. Sarker. Effect of GGBFS on setting, workability and early strength properties of fly ash geopolymer concrete cured in ambient condition. Construction and Building Materials, Vol. 66, 2014, pp. 163-171.
- Xie, J., J. Wang, R. Rao, C. Wang, and C. Fang. Effects of combined [62] usage of GGBS and fly ash on workability and mechanical properties of alkali activated geopolymer concrete with recycled aggregate. Composites Part B: Engineering, Vol. 164, No. Jun 2018, 2019, pp. 179-190.
- [63] Rafeet, A., R. Vinai, M. Soutsos, and W. Sha. Guidelines for mix proportioning of fly ash/GGBS based alkali activated concretes. Construction and Building Materials, Vol. 147, 2017, pp. 130-142.
- [64] Jang, J. G., N. K. Lee, and H. K. Lee. Fresh and hardened properties of alkali-activated fly ash/slag pastes with superplasticizers. Construction and Building Materials, Vol. 50, 2014, pp. 169-176.
- [65] Deb, P. S., P. Nath, and P. K. Sarker. The effects of ground granulated blast-furnace slag blending with fly ash and activator content on the workability and strength properties of geopolymer concrete cured at ambient temperature. Materials & Design, Vol. 62, 2014, pp. 32-39.
- [66] Yang, K. H., J. K. Song, A. F. Ashour, and E. T. Lee. Properties of cementless mortars activated by sodium silicate. Construction and Building Materials, Vol. 22, No. 9, 2008, pp. 1981-1989.
- Gao, X., Q. L. Yu, and H. J. H. Brouwers. Characterization of alkali [67] activated slag-fly ash blends containing nano-silica. Construction and Building Materials, Vol. 98, 2015, pp. 397-406.
- Nuaklong, P., V. Sata, and P. Chindaprasirt. Influence of recycled [68] aggregate on fly ash geopolymer concrete properties. Journal of Cleaner Production, Vol. 112, 2016, pp. 2300-2307.
- [69] Malkawi, A. B., M. F. Nuruddin, A. Fauzi, H. Almattarneh, and B. S. Mohammed. Effects of Alkaline Solution on Properties of the HCFA Geopolymer Mortars. Procedia Engineering, Vol. 148, 2016,
- Görhan, G. and G. Kürklü. The influence of the NaOH solution on [70] the properties of the fly ash-based geopolymer mortar cured at different temperatures. Composites Part B: Engineering, Vol. 58, 2014, pp. 371-377.
- [71] Lemougna, P. N., A. Nzeukou, B. Aziwo, A. B. Tchamba, K. T. Wang, U. C. Melo, et al. Effect of slag on the improvement of setting time and compressive strength of low reactive volcanic ash geopolymers synthetized at room temperature. Materials Chemistry and Physics, Vol. 239, No. Aug 2019, 2020, id. 122077.

- [72] ASTM C150/C150M-15. Standard Specification for Portland Cement. ASTM International, West Conshohocken, PA, 2015.
- [73] Kumar, S., R. Kumar, and S. P. Mehrotra. Influence of granulated blast furnace slag on the reaction, structure and properties of fly ash based geopolymer. *Journal of Materials Science*, Vol. 45, No. 3, 2010, pp. 607–615.
- [74] Wang, W. C., H. Y. Wang, and M. H. Lo. The fresh and engineering properties of alkali activated slag as a function of fly ash replacement and alkali concentration. *Construction and Building Materials*, Vol. 84, 2015, pp. 224–229.
- [75] Wang, Y., R. Xiao, W. Hu, X. Jiang, X. Zhang, and B. Huang. Effect of granulated phosphorus slag on physical, mechanical and microstructural characteristics of Class F fly ash based geopolymer. Construction and Building Materials, Vol. 291, 2021, id. 123287.
- [76] Samantasinghar, S. and S. P. Singh. Effect of synthesis parameters on compressive strength of fly ash-slag blended geopolymer. *Construction and Building Materials*, Vol. 170, 2018, pp. 225–234.
- [77] Patel, Y. J. and N. Shah. Enhancement of the properties of Ground Granulated Blast Furnace Slag based Self Compacting Geopolymer Concrete by incorporating Rice Husk Ash. Construction and Building Materials, Vol. 171, 2018, pp. 654–662.
- [78] Nath, P. and P. K. Sarker. Flexural strength and elastic modulus of ambient-cured blended low-calcium fly ash geopolymer concrete. Construction and Building Materials, Vol. 130, 2017, pp. 22–31.
- [79] Tang, Z., Y. Hu, V. W. Y. Tam, and W. Li. Uniaxial compressive behaviors of fly ash/slag-based geopolymeric concrete with recycled aggregates. *Cement and Concrete Composites*, Vol. 104, 2019, id. 103375.
- [80] Kumar, G. and S. S. Mishra. Effect of GGBFS on workability and strength of alkali-activated geopolymer concrete. *Civil Engineering Journal*, Vol. 7, No. 6, 2021, pp. 1036–1049.
- [81] Nath, P. and P. K. Sarker. Fracture properties of GGBFS-blended fly ash geopolymer concrete cured in ambient temperature. *Mater Struct*, Vol. 5050 2017, id. 32.
- [82] Hu, Y., Z. Tang, W. Li, Y. Li, and V. W. Y. Tam. Physical-mechanical properties of fly ash/GGBFS geopolymer composites with recycled aggregates. *Construction and Building Materials*, Vol. 226, 2019, pp. 139–151.
- [83] Puligilla, S. and P. Mondal. Role of slag in microstructural development and hardening of fly ash-slag geopolymer. Cement and Concrete Research, Vol. 43, 2013, pp. 70–80.
- [84] Ismail, I., S. A. Bernal, J. L. Provis, R. San Nicolas, S. Hamdan, and J. S. J. van Deventer. Modification of phase evolution in alkaliactivated blast furnace slag by the incorporation of fly ash. *Cement and Concrete Composites*, Vol. 45, 2014, pp. 125–135.
- [85] Dehghani, A., F. Aslani, Ghaebi, and N. Panah. Effects of initial SiO<sub>2</sub>/Al<sub>2</sub>O<sub>3</sub> molar ratio and slag on fly ash-based ambient cured geopolymer properties. *Construction and Building Materials*, Vol. 293, 2021, id. 123527.
- [86] Yip, C. K., G. C. Lukey, J. L. Provis, and J. S. J. van Deventer. Effect of calcium silicate sources on geopolymerisation. *Cement and Concrete Research*, Vol. 38, No. 4, 2008, pp. 554–564.
- [87] Temuujin, J., A. van Riessen, and R. Williams. Influence of calcium compounds on the mechanical properties of fly ash geopolymer pastes. *Journal of Hazardous Materials*, Vol. 167, No. 1, 2009, pp. 82–88.
- [88] Zhang, Z. Q. and H. Y. Wu. Rate of the miniemulsion polymerization costabilized by pre-polymer PMMA. Gao Xiao Hua Xue Gong

- Cheng Xue Bao/Journal of Chemical Engineering of Chinese Universities, Vol. 23, No. 1, 2009, pp. 75–79.
- [89] Chindaprasirt, P., C. Jaturapitakkul, W. Chalee, and U. Rattanasak. Comparative study on the characteristics of fly ash and bottom ash geopolymers. Waste Management (New York, N.Y.), Vol. 29, No. 2, 2009, pp. 539–543.
- [90] Álvarez-Ayuso, E., X. Querol, F. Plana, A. Alastuey, N. Moreno, M. Izquierdo, et al. Environmental, physical and structural characterisation of geopolymer matrixes synthesised from coal (co-) combustion fly ashes. *Journal of Hazardous Materials*, Vol. 154, No. 1–3, 2008, pp. 175–183.
- [91] Panias, D., I. P. Giannopoulou, and T. Perraki. Effect of synthesis parameters on the mechanical properties of fly ash-based geopolymers. *Colloids and Surfaces A: Physicochemical and Engineering Aspects*, Vol. 301, No. 1–3, 2007, pp. 246–254.
- [92] Fernández-Jiménez, A. and A. Palomo. Composition and microstructure of alkali activated fly ash binder: Effect of the activator. *Cement and Concrete Research*, Vol. 35, No. 10, 2005, pp. 1984–1992.
- [93] Komnitsas, K. and D. Zaharaki. Geopolymerisation: A review and prospects for the minerals industry. *Minerals Engineering*, Vol. 20, No. 14, 2007, pp. 1261–1277.
- [94] Dimas, D. D., I. P. Giannopoulou, and D. Panias. Utilization of alumina red mud for synthesis of inorganic polymeric materials. *Mineral Processing & Extractive Metallurgy Review*, Vol. 30, No. 3, 2009, pp. 211–239.
- [95] Marjanović, N., M. Komljenović, Z. Baščarević, V. Nikolić, and R. Petrović. Physical-mechanical and microstructural properties of alkali-activated fly ash-blast furnace slag blends. *Ceramics International*, Vol. 41, No. 1, 2015, pp. 1421–1435.
- [96] Yip, C. K. and J. S. J. Van Deventer. Microanalysis of calcium silicate hydrate gel formed within a geopolymeric binder. *Journal of Materials Science*, Vol. 38, No. 18, 2003, pp. 3851–3860.
- [97] Nie, Q., W. Hu, T. Ai, B. Huang, X. Shu, and Q. He. Strength properties of geopolymers derived from original and desulfurized red mud cured at ambient temperature. *Construction and Building Materials*, Vol. 125, 2016, pp. 905–911.
- [98] Puertas, F., M. Palacios, H. Manzano, J. S. Dolado, A. Rico, and J. Rodríguez. A model for the C-A-S-H gel formed in alkali-activated slag cements. *Journal of the European Ceramic Society*, Vol. 31, No. 12, 2011, pp. 2043–2056.
- [99] Gebregziabiher, B. S., R. Thomas, and S. Peethamparan. Very early-age reaction kinetics and microstructural development in alkali-activated slag. *Cement and Concrete Composites*, Vol. 55, 2015, pp. 91–102.
- [100] Al-Majidi, M. H., A. Lampropoulos, A. Cundy, and S. Meikle. Development of geopolymer mortar under ambient temperature for in situ applications. *Construction and Building Materials*, Vol. 120, 2016, pp. 198–211.
- [101] Yu, P., R. J. Kirkpatrick, B. Poe, P. F. McMillan, and X. Cong. Structure of Calcium Silicate Hydrate (C-S-H): Near-, Mid-, and Far-Infrared Spectroscopy. *Journal of the American Ceramic Society*, Vol. 82, No. 3, 1999 Mar, pp. 742–748.
- [102] Ahmed, S., T. Meng, and M. Taha. Utilization of red mud for producing a high strength binder by composition optimization and nano strengthening. *Nanotechnology Reviews*, Vol. 9, No. 1, 2020, pp. 396–409.
- [103] Kaze, C. R., J. N. Y. Djobo, A. Nana, H. K. Tchakoute, E. Kamseu, U. C. Melo, et al. Effect of silicate modulus on the setting, mechanical

- strength and microstructure of iron-rich aluminosilicate (laterite) based-geopolymer cured at room temperature. Ceramics International, Vol. 44, No. 17, 2018, pp. 21442-21450.
- [104] Bernal, S. A., J. L. Provis, V. Rose, and R. Mejía De Gutierrez. Evolution of binder structure in sodium silicate-activated slagmetakaolin blends. Cement and Concrete Composites, Vol. 33, No. 1,
- [105] Criado, M., A. Palomo, and A. Fernández-liménez, Alkali activation of fly ashes. Part 1: Effect of curing conditions on the carbonation of the reaction products. Fuel, Vol. 84, No. 16, 2005, pp. 2048-2054.
- Strydom, C. A. and J. C. Swanepoel. Utilisation of fly ash in a geopolymeric material. Applied Geochemistry, Vol. 17, No. 8, 2002,
- [107] Zhang, Z., H. Wang, J. L. Provis, F. Bullen, A. Reid, and Y. Zhu. Quantitative kinetic and structural analysis of geopolymers. Part 1. the activation of metakaolin with sodium hydroxide. Thermochimica Acta. THA, Vol. 539, 2012, pp. 23-33.
- [108] Peng, H., C. Cui, Z. Liu, C. S. Cai, and Y. Liu. Synthesis and reaction mechanism of an alkali-activated metakaolin-slag composite system at room temperature. Journal of Materials in Civil Engineering, Vol. 31, No. 1, 2019 Jan, id. 4018345.
- [109] Wetzel, A. and B. Middendorf. Influence of silica fume on properties of fresh and hardened ultra-high performance concrete based on alkali-activated slag. Cement and Concrete Composites, Vol. 100, No. Mar, 2019, pp. 53-59.
- [110] Torres-Carrasco, M., C. Rodríguez-Puertas, M. Del Mar Alonso, and F. Puertas. Alkali activated slag cements using waste glass as alternative activators. Rheological behaviour. Boletín de la sociedad española de Ceramica y Vidrio, Vol. 54, No. 2, 2015, pp. 45-57.
- Tchakouté, H. K., C. H. Rüscher, E. Kamseu, J. N. Y. Djobo, and C. Leonelli. The influence of gibbsite in kaolin and the formation of berlinite on the properties of metakaolin-phosphate-based geopolymer cements. Materials Chemistry and Physics, Vol. 199, 2017,
- Samantasinghar, S. and S. P. Singh. Red mud-slag blends as a sustainable road construction material. Construction and Building Materials, Vol. 375, 2023, id. 130926.
- Mukiza, E., L. L. Zhang, X. Liu, and N. Zhang. Utilization of red mud in road base and subgrade materials: A review. Resources,

- Conservation and Recycling, Vol. 141, No. Jun 2018, 2019, pp. 187-199.
- [114] Mukiza, E., X. Liu, L. Zhang, and N. Zhang. Preparation and characterization of a red mud-based road base material: Strength formation mechanism and leaching characteristics. Construction and Building Materials, Vol. 220, 2019, pp. 297-307.
- Kim, Y., Y. Lee, M. Kim, and H. Park. Preparation of high porosity bricks by utilizing red mud and mine tailing. Journal of Cleaner Production, Vol. 207, 2019, pp. 490-497.
- [116] Panias, D., I. Giannopoulou, and D. Boufounos. Valorization of alumina red mud for production of geopolymeric bricks and tiles. Light Metals, Vol. 2014, No. 9781118889, 2014, pp. 155-159.
- [117] Pontikes, Y. and G. N. Angelopoulos. Effect of firing atmosphere and soaking time on heavy clay ceramics with addition of Bayer's process bauxite residue. Advances in Applied Ceramics, Vol. 108, No. 1, 2009, pp. 50-56.
- [118] Scribot, C., W. Maherzi, M. Benzerzour, Y. Mamindy-Pajany, and N. E. Abriak. A laboratory-scale experimental investigation on the reuse of a modified red mud in ceramic materials production. Construction and Building Materials, Vol. 163, 2018, pp. 21–31.
- Wagh, A. S. and V. E. Douse. Silicate bonded unsintered ceramics of Bayer process waste. Journal of Materials Research, Vol. 6, No. 5, 1991, pp. 1094-1102.
- [120] Pérez-Villarejo, L., F. A. Corpas-Iglesias, S. Martínez-Martínez, R. Artiaga, and J. Pascual-Cosp. Manufacturing new ceramic materials from clay and red mud derived from the aluminium industry. Construction and Building Materials, Vol. 35, 2012, pp. 656-665.
- [121] Chen, X., A. Lu, and G. Qu. Preparation and characterization of foam ceramics from red mud and fly ash using sodium silicate as foaming agent. Ceramics International, Vol. 39, No. 2, 2013,
- [122] Mandal, A. K., H. R. Verma, and O. P. Sinha. Utilization of aluminum plant's waste for production of insulation bricks. Journal of Cleaner Production, Vol. 162, 2017, pp. 949-957.
- [123] Ghalehnovi, M., E. Asadi Shamsabadi, A. Khodabakhshian, F. Sourmeh, and J. de Brito. Self-compacting architectural concrete production using red mud. Construction and Building Materials, Vol. 226, 2019, pp. 418-427.